The Cryosphere

Early Holocene ice on the Begguya plateau (Mt. Hunter, Alaska) revealed by ice core ^{14}C age constraints

Ling Fang[1,a]**, Theo M. Jenk**[1,3]**, Dominic Winski**[4]**, Karl Kreutz**[4]**, Hanna L. Brooks**[4]**, Emma Erwin**[4]**, Erich Osterberg**[5]**, Seth Campbell**[4]**, Cameron Wake**[6]**, and Margit Schwikowski**[1,2,3]

[1]Laboratory for Environmental Chemistry, Paul Scherrer Institute, 5232 Villigen PSI, Switzerland
[2]Department of Chemistry and Biochemistry, University of Bern, 3012 Bern, Switzerland
[3]Oeschger Centre for Climate Change Research, University of Bern, 3012 Bern, Switzerland
[4]Climate Change Institute and School of Earth and Climate Science, University of Maine, Orono, ME 04469, USA
[5]Department of Earth Sciences, Dartmouth College, Hanover, NH 03755, USA
[6]Institute for the Study of Earth, Oceans, and Space, University of New Hampshire, Durham, NH 03824, USA
[a]present address: Shaanxi Key Laboratory of Earth Surface System and Environmental Carrying Capacity, Urban and
Environmental Sciences Department, Northwest University, Xi'an 710127, China

Correspondence: Theo M. Jenk (theo.jenk@psi.ch)

Abstract. Investigating North Pacific climate variability during warm intervals prior to the Common Era can improve our understanding of the behavior of ocean–atmosphere teleconnections between low latitudes and the Arctic under future warming scenarios. However, most of the existing ice core records from the Alaskan and Yukon region only allow access to climate information covering the last few centuries. Here we present a surface-to-bedrock age scale for a 210 m long ice core recovered in 2013 from the summit plateau of Begguya (Mt. Hunter; Denali National Park, Central Alaska). Combining dating by annual layer counting with absolute dates from micro-radiocarbon dating, a continuous chronology for the entire ice core archive was established using an ice flow model. Calibrated ^{14}C ages from the deepest section (209.1 m, 7.7 to 9.0 ka cal BP) indicate that basal ice on Begguya is at least of early Holocene origin. A series of samples from a shallower depth interval (199.8 to 206.6 m) were dated with near-uniform ^{14}C ages (3 to 5 ka cal BP). Our results suggest this may be related to an increase in annual net snow accumulation rates over this period following the Northern Hemisphere Holocene Climate Optimum (around 8 to 5 kyr BP). With absolute dates constraining the timescale for the last > 8 kyr BP, this paleo-archive will allow future investigations of Holocene climate and the regional evolution
of spatial and temporal changes in atmospheric circulation and hydroclimate in the North Pacific.

1 Introduction

Arctic surface temperatures have increased more than twice as fast as global temperature during the early 20th century and since the 1970s (Bengtsson et al., 2004; Tokinaga et al., 2017; Svendsen et al., 2018). Recent modeling results suggest that during the early 20th century, as the Pacific Decadal Oscillation (PDO) transitioned to a positive phase, there was a concomitant deepening of the Aleutian Low that warmed the Arctic through poleward low-level advection of extratropical air (Svendsen et al., 2018). The impact of Pacific multidecadal variability on Arctic warming has considerable implications for sea ice extent (Screen and Francis, 2016) and hence the possible linkage between Arctic amplification, sea ice loss, and enhanced midlatitude winter variability (Cohen et al., 2014, 2018, 2019; Francis et al., 2017; Screen et al., 2018; Blackport et al., 2019). Whether the present positive PDO conditions will persist and contribute to Arctic warming at an even higher rate in the future remains a fundamental question (Svendsen et al., 2018). A longer-term perspective on Pacific decadal variability and the teleconnection between

the tropical Pacific, North Pacific, and the Arctic, particularly during warm intervals in the Holocene outside those captured in the instrumental record, would be an important contribution to this problem (e.g., Park et al., 2019). High-mountain ice cores in the North Pacific region have the advantage of sampling atmospheric moisture (e.g., snow) and aerosol deposition, as well as preserving physical characteristics (e.g., melt), all of which can be related to Pacific climate processes (Zdanowicz et al., 2014; Osterberg et al., 2017; Winski et al., 2018) if Holocene (or greater) length records can be recovered.

The general timing of deglaciation in Alaska (Brooks Range, Central Alaska Range, and southern Alaska) was determined based on terrestrial cosmogonic radionuclides, lichenometry, and radiocarbon dating to between 10 and 20 kyr BP (Dortch, 2007). Following the Last Glacial Maximum (LGM), glaciers in the Brooks Range retreated up valley to, or even within, their modern limits by ca. 15 ka (Pendleton et al., 2015). Given the small extent of the Brooks Range glaciers prior to the Holocene thermal maximum, during which some glaciers in southern Alaska disappeared entirely (Barclay et al., 2009), it is possible that the Brooks Range glaciers may have disappeared as well. In the Central Alaska Range, reaching much higher altitudes and considering today's glacier extent, this is rather unlikely. Nevertheless, it is unclear where preserved ice from the early Holocene (or older) can be found in basal layers of these glaciers. Most of the ice cores recovered from the Alaskan and Yukon region did not reach bedrock and are thus limited in the time covered, reaching back a few centuries only (Fig. 1). The Prospector-Russell Col (PRCol) ice core from Mt. Logan is an exception, having an estimated bottom age of ~ 20 kyr BP based on the assumption that the significant depletion in the water stable isotope ratios observed in the very bottom section of the core is a signal of the LGM cold conditions (Fisher et al., 2008). The PRCol chronology is further constrained by a large δ^{18}O minimum and coeval increases in deuterium excess and Ca^{2+}, which are assigned to the 4.2 ka BP event (Walker et al., 2019), as well as tephra from the large Alaskan eruption of Aniakchak (3.6 kyr BP; Walker et al., 2019). The PRCol record serves as a global auxiliary stratotype for the Middle and Late Holocene subdivision boundary (Walker et al., 2019). However, there are no chronologic tie points in the PRCol record prior to the 4.2 ka BP event (Walker et al., 2019).

New surface-to-bedrock ice cores were recovered from the Begguya plateau (Mt. Hunter; Denali National Park, Alaska; 62.93° N, 151.09° W; Fig. 1) in 2013 at 3900 m elevation (Winski et al., 2017). The two surface-to-bedrock cores (DEN-13A, DEN-13B) reached depths of 211.2 and 209.7 m, respectively. Analysis of the upper 190 m of DEN-13B (2013 to 810 CE) revealed that snow accumulation at the drilling site has doubled since ~ 1840 CE, coeval with the warming of western tropical Pacific sea surface temperatures (Winski et al., 2017) and intensification of the Aleutian Low

system (Osterberg et al., 2014, 2017). The same core also shows a 60-fold increase in water equivalent of total annual melt between 1850 CE and present, which suggests a summer warming rate of 1.92 ± 0.31 °C per century during the last 100 years in the altitude range of 3900 m (Winski et al., 2018). The Begguya melt layer record is significantly correlated with surface temperatures in the central tropical Pacific through a Rossby-wave-like pattern that enhances temperatures over Alaska (Winski et al., 2018). Taken together, these hydroclimate changes are consistent with linkages between Pacific decadal variability and Arctic hydroclimate changes seen in the observational record (Svendsen et al., 2018), and they demonstrate that the North Pacific hydroclimate response since 1850 CE is unprecedented in the past millennium.

The annual layer-counting-based chronology of the Denali core results in an ice age of 1203 ± 41 years at a depth of 190 m (152.8 m w.e., water equivalent; Winski et al., 2017). Below that depth, annual layering was less consistent due to the loss of seasonal resolution caused by the glacier-flow-induced thinning of layers. However, based on previously reported age–depth scales of ice cores from cold, high-elevation glaciers frozen to bedrock, the bottom 20 m of ice may contain most of the record in terms of time, covering the Holocene and potentially even reaching into the Last Glacial period (Uglietti et al., 2016; Licciulli et al., 2020). The Denali ice core therefore provides the possibility of establishing a new Holocene North Pacific hydroclimate record reaching beyond the Common Era if a precise and absolute-dated chronology can be established in the bottom 20 m of the core. The water-insoluble organic carbon (WIOC) and dissolved organic carbon (DOC) ^{14}C dating method has been validated and applied for multiple midlatitude ice cores (e.g., Jenk et al., 2009; Uglietti et al., 2016; Hou et al., 2018; Fang et al., 2021). The technique makes use of the transport and deposition of carbonaceous aerosols onto the glacier. Before the industrial period, carbonaceous aerosols were mainly emitted from the living biosphere and from biomass burning. Consequently, this carbon reflects the contemporary atmospheric ^{14}C content (Jenk et al., 2006). After deposition, the WIOC and DOC are incorporated into glacier snow, firn, and ice and undergo radioactive decay with a half-life of 5730 years (Godwin, 1962). Here we report results from ^{14}C analysis of the bottom 60 m of the Denali ice core. These absolute dates extend the existing late Holocene Begguya chronology (Winski et al., 2017), providing the first high-latitude Northern Hemisphere ice core chronology based on absolute dates from radiometric methods. We discuss our results in relation to Holocene ice extent and climate in the North Pacific region.
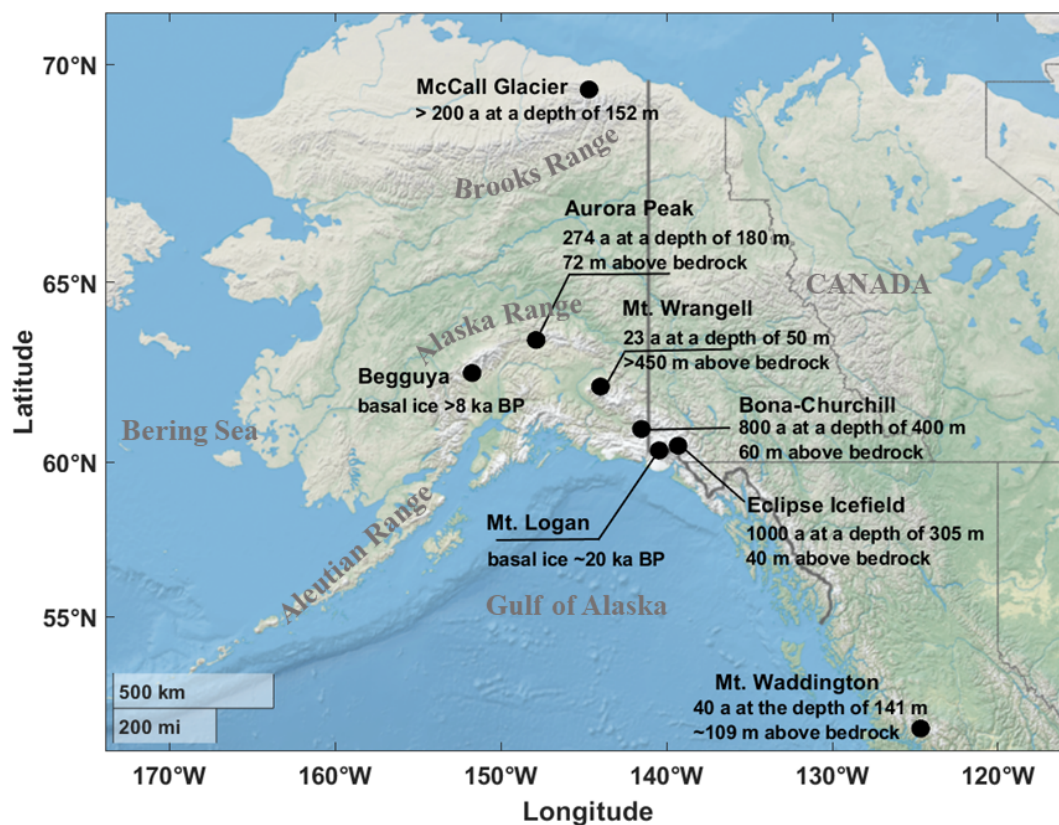
Figure 1. Location map of North Pacific ice core sites and the age of the oldest ice dated from each location: Begguya (Mt. Hunter; this study), McCall Glacier (Klein et al., 2016), Aurora Peak (Tsushima, 2015), Mt. Wrangell (Yasunari et al., 2007), Bona-Churchill (Porter et al., 2019), Mt. Logan (Fisher et al., 2008), Eclipse Icefield (Yalcin et al., 2007), and Mt. Waddington (Neff et al., 2012).

2 Methods

2.1 Annual layer counting

Two surface-to-bedrock ice cores (DEN-13A, DEN-13B) were drilled in 2013 at 3900 m elevation above sea level (a.s.l.) from the saddle between the north and middle peaks of Begguya (Mt. Hunter), Alaska (Winski et al., 2017, 2018; Osterberg et al., 2017; Polashenski et al., 2018). The annual layer counting for DEN-13B was previously published (Winski et al., 2017) and is only briefly described here. The timescale from 2013 to 1777 CE was determined by counting annual oscillations in $\delta^{18}O$ (summer peak), melt layers (summer peak), magnesium (spring peak), dust (spring peak), liquid conductivity (summer peak), ammonium (summer peak), and methanesulfonic acid (MSA; late summer–fall peak), consistent with previous North Pacific ice cores (Yasunari et al., 2007; Osterberg et al., 2014; Tsushima et al., 2015). Between 1777 and 1500 CE annual layer counting is based on annual oscillations of $\delta^{18}O$, δD, dust concentration, and liquid conductivity that were measured at higher resolution than the other analytes, while conductivity and dust concentrations were exclusively used to date the ice core from 1500 back to 810 CE. For this study, the counting based on

these two parameters has been extended back in time (see Sect. 3.2).

2.2 Denali ice core ^{14}C analysis

A total of 16 samples were selected from the lower portion of DEN-13B (Table 1). Because WIOC concentrations at this site were assumed to be low, ice samples of at least 1 kg of mass were cut, aiming for extracted yields of carbon that allow dating with a reasonable uncertainty of 10 %–20 % ($> 10\,\mu g\,C$; Uglietti et al., 2016). In order to process such large sample volumes, a splitting of the sample for melting was required and the overall filtration time had to be increased. Using artificial ice produced from ultra-pure water, the adapted procedures were tested to reach low blanks similar to the ones previously achieved for smaller samples (Jenk et al., 2009; Uglietti et al., 2016; Fang et al., 2019). Otherwise, the samples for WIOC ^{14}C dating were prepared following the protocol described in Uglietti et al. (2016) with a brief summary provided here. In order to remove potential contamination in the outer layer of the ice core, pre-cut samples from the inner part of the core were rinsed with ultra-pure water. After the melting of the sample in a pre-cleaned jar (1 L, PETG, Semadeni), due to the size split in two, the

Table 1. The ^{14}C results of the Denali ice core samples (DEN-13B), given as F^{14}C, ^{14}C ages, and calibrated ^{14}C ages. For ^{14}C calibration, chronological layering was assumed (sequential deposition; see main text). Samples were dated using the WIOC fraction, except for section 235 in which the DOC fraction was analyzed. Numbers of the carbon amount available for ^{14}C AMS analysis as well as the concentration of WIOC (DOC) in the sample are also provided. Additionally shown is the range of the dating based on ALC (range from top to bottom depth of section) and the final age scale (inverse ice flow model; provided is the uncertainty range at mid-depth of the analyzed section).

Sample ID	AMS lab ID	Depth (m)	Mid-depth (m w.e.)	Carbon amount (µg C)	WIOC (µg C kg^{-1})	F^{14}C (1σ)	^{14}C age (yr BP, 1σ)	Calibrated ^{14}C age (yr cal BP, 1σ range)	Final age at mid-depth (yr BP)	ALC scale (yr BP)
Denali164	BE-10013.1.1	148.6–149.4	115.90	7	6.2	0.910 ± 0.058	758 ± 513	–[a]	160–180	150–180
Denali183	BE-10015.1.1	165.7–166.6	131.40	11	10.1	0.921 ± 0.042	661 ± 367	4–679	350–370	340–380
Denali209	BE-10016.1.1	187.8–188.7	151.16	9	9.8	0.826 ± 0.044	1536 ± 428	–[a]	1010–1060	980–1090
Denali210-211	BE-8997.1.1	188.7–190.3	152.29	11	20.0	0.922 ± 0.033	652 ± 288	527–930	1080–1130	1030–1190
Denali214	BE-10017.1.1	192.1–192.9	155.00	14	11.8	0.831 ± 0.036	1487 ± 348	958–1410	1160–1420	1230–1380
Denali215-216	BE-8998.1.1	193.0–194.7	156.17	9	12.0	0.925 ± 0.039	626 ± 339	–[a]	1200–1560	1290–1560
Denali217	BE-10018.1.1	194.7–195.5	157.33	7	6.1	0.731 ± 0.054	2517 ± 594	–[a]	1280–1710	1400–1560
Denali219-220	BE-8615.1.1	196.4–197.3	159.31	12	16.8	0.841 ± 0.026	1391 ± 248	1242–1706	1560–1970	> 1420
Denali223	BE-10019.1.1	199.8–200.7	161.93	21	17.3	0.608 ± 0.029	3997 ± 383	3079–3469	2180–2890	–
Denali224-225	BE-11923.1.1	200.7–202.3	163.06	34	17.5	0.653 ± 0.010	3423 ± 123	3257–3530	2470–3510	–
Denali228	BE-10020.1.1	203.5–204.2	165.11	9	10.0	0.627 ± 0.043	3750 ± 552	–[a]	2860–3850	–
Denali229-230	BE-11924.1.1	204.2–205.7	166.09	39	20.0	0.691 ± 0.009	2969 ± 105	3305–3566	3040–4040	–
Denali231	BE-10021.1.1	205.7–206.6	167.18	11	11.5	0.523 ± 0.037	5207 ± 569	3840–4263	3540–4560	–
Denali232-233	BE-11925.1.1	206.6–208.1	168.26	55	30.8	0.629 ± 0.008	3724 ± 102	4067–4407	4520–5430	–
Denali234	BE-10022.1.1	208.1–208.8	169.23	10	11.7	0.378 ± 0.043	7814 ± 918	7264–8406	6270–9650	–
Denali235[b]	BE-12465.1.1	208.8–209.4	169.83	21	80.3$_{DOC}$	(0.437 ± 0.025)	(6649 ± 447)			
						0.418 ± 0.027[c]	7007 ± 520	7737–8987[c]	8920–13140	–

[a] Following recommendations, samples with a carbon mass of significantly less than 10 µg C were not considered (Uglietti et al., 2016). [b] Results from the DOC fraction. [c] After correction for in situ ^{14}C production (Fang et al., 2021; see main text).

carbonaceous particles contained as impurities in the sample ice were filtered onto a prebaked quartz fiber filter (Pallflex Tissuquartz 2500QAT-UP). Potential particulate carbonates also remaining on the filter were removed by acidifying three times with 0.5 µL of 0.2 M HCl. These initial steps were performed in a class 100 laminar flow box to ensure clean conditions. At the University of Bern (Laboratory for the Analysis of Radiocarbon with AMS – accelerator mass spectrometer – LARA laboratory) the WIOC samples were then combusted in a thermo-optical OC/EC (organic carbon and elemental carbon) analyzer (Sunset Modeldoc4L, Sunset Laboratory Inc, USA) with a non-dispersive infrared sensor for CO_2 quantification, using the established Swiss 4S protocol for OC/EC separation (Zhang et al., 2012). Being coupled to a 200 kV compact accelerator mass spectrometer (AMS, mini radiocarbon dating system MICADAS), equipped with a gas ion source and a gas interface system (GIS; Ruff et al., 2007; Synal et al., 2007; Szidat et al., 2014), the LARA Sunset–GIS–AMS system (Agrios et al., 2015, 2017) allowed for final, online ^{14}C measurements of the CO_2 produced from the WIOC fraction.

For the deepest sample from ∼ 209 m depth (Denali235) the available amount of ice was very limited (∼ 200 g). To ensure a sufficient mass of carbon for final AMS analysis, the ^{14}C dating was performed on the DOC fraction, for which a higher concentration compared to the WIOC fraction is expected (Legrand et al., 2013). By a catalyzed UV oxidation in a dedicated system, DOC was converted to CO_2 which was then cryogenically trapped and flame sealed in glass am-

pules for final AMS analysis. Details can be found in Fang et al. (2019).

All ^{14}C results are expressed as fraction modern (F^{14}C), which is the ^{14}C / ^{12}C ratio of the sample divided by the same ratio of the modern standard referenced to the year 1950 CE (NIST standard oxalic acid II, SRM 4990C), both being normalized to −25‰ in δ^{13}C to account for isotopic fractionation. Daily AMS calibration was performed using sets of modern (NIST oxalic acid II, SRM 4990C, F^{14}C = 1.3407 ± 0.0005) and fossil standards (sodium acetate, Sigma-Aldrich, no. 71180, F^{14}C = 0.0018 ± 0.0005). Final values presented in Table 1 are the AMS F^{14}C raw data after corrections accounting for constant contamination and cross contamination in the Sunset–GIS–AMS system (or GIS–AMS system for DOC, respectively) and the overall procedural blank contribution introduced from the preparation of ice samples to final AMS analysis. F^{14}C of DOC was corrected for the contribution from ^{14}C in situ production following Fang et al. (2021). The applied small shift in F^{14}C of 0.019 ± 0.010 was derived using an in situ production rate of 260.9 ^{14}C atoms g_{ice}^{-1} yr^{-1} as the best estimate for the site latitude and elevation (Lal et al., 1987; Lal and Jull, 1990; Lal, 1992), an average accumulation rate of 1.0 ± 0.5 m w.e. (a best initial guess based on the annual values from Winski et al., 2017, ranging from 0.2 to 2.0 m w.e. for the time period 810 to 2013 CE), and assuming an average incorporation into DOC of 18 ± 7 % (Hoffmann, 2016). This correction shifts the calibrated age to be 300 ± 200 years older, with uncertainty being fully propagated as for all other ages. Note that

the upper estimate does not exceed the achieved dating precision defined by the analytical uncertainty (see Table S1 in the Supplement). For all samples, calibrated radiocarbon ages were derived by calibrating final $F^{14}C$ values using OxCal v4.4.4 (Ramsey, 2021) with IntCal20 (the Northern Hemisphere calibration curve; Reimer et al., 2020) and the OxCal in-built sequence model (Bayesian-approach-based deposition model; Ramsey, 2008, 2017). All calibrated ^{14}C ages are presented as the 1σ range in years before present (cal BP, with BP referring to the year 1950 CE).

3 Results

3.1 Englacial stratigraphy

Around the Begguya drill site, no folding was observed in ground-penetrating radar (GPR) data, and the bedrock geometry appears to be uncomplicated (Campbell et al., 2013). New radar data were collected in 2022. Ice thickness, bed topography, and internal stratigraphy of the core site were mapped using GPR (10 MHz center frequency radar system, Blue Systems Integration). Standard processing techniques were applied to the data: clipping stationary periods, applying horizontal stacking, bandpass filtering, and correction for antenna separation (Lilien et al., 2020). Data were interpolated for standard trace spacing and then migrated using the SeisUnix sumigtk routine. Clear, visible layering is evident in the majority of the ice column; however, the interpretation of the stratigraphy at depth is complicated by sidewall reflections produced from the trough beneath the ice core site. There is no conclusive evidence from these data of either stratigraphic continuity or discontinuity in the bottom-most 10 m of ice (Fig. 2). Future measurements using the millimeter-precision capabilities of autonomous phase-sensitive radar (Brennan et al., 2014) would be beneficial to resolve englacial stratigraphy close to the bedrock.

3.2 Annual layer counting

Annual layer counting (ALC), previously published in Winski et al. (2017) back to 810 CE (Sect. 2.1.), was extended back to 339 CE, i.e., for the top 197 m. The uncertainty in the ALC chronology back to 810 CE was estimated through statistical comparisons among individual layer positions indicated by three individuals (see Winski et al., 2017, for details). By 1900 CE, uncertainty estimates are ± 4 years, increasing to ± 10 years at 1500 CE and ± 30 years by 810 CE (190.05 m). Only one individual (DW) performed ALC below 190 m, prohibiting a similar approach to estimate uncertainties, but we estimate an uncertainty of around ± 60 years at 339 CE. These estimates are for ALC only and do not consider additional, constraining information from time horizons. There is no offset between the timescale and inferred volcanic eruptions as indicated by peaks in sulfate, chloride, and conductivity during the 19th and 20th centuries, indi-
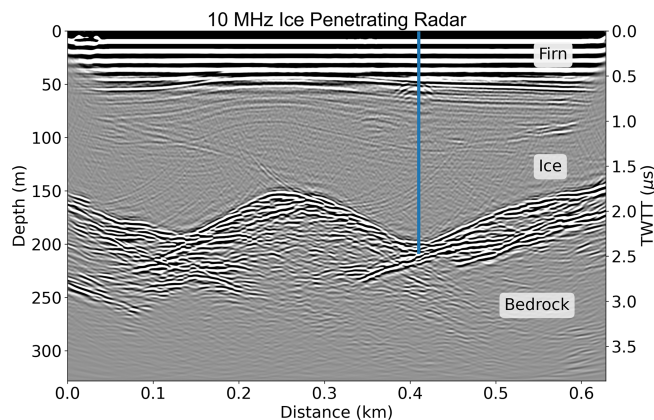

Figure 2. Ground-penetrating radar profile collected with 10 MHz BSI radar across the Begguya plateau in 2022. Standard processing techniques were applied to the data using ImpDAR (Lilien et al., 2020). The two-way travel time (TWTT) is plotted on the y axis on the right side. The Denali ice core drilling (DEN-13B) is indicated by the vertical blue line.

cating that an accuracy within ± 2 years throughout the last 200 years is likely. The sulfate and chloride peaks in the 18th century used for chronology validation (inferred as Laki, 1784 CE, and Pavlof, 1763 CE) were offset by 1 year from the ALC chronology. Additionally, ^{137}Cs concentrations in the Denali core strongly peak in the layer assigned to the year 1963 CE, 1 year after the most extensive atmospheric testing of nuclear weapons, which matches the ^{137}Cs residence time in the atmosphere (Tian et al., 2007; Winski et al., 2017).

3.3 Denali ice core ^{14}C data

Air masses leading to precipitation on Begguya ($\sim$ 3900 m a.s.l.) originate predominantly from the Pacific and contain relatively low organic aerosol concentrations (Haque et al., 2016; Choi et al., 2017). The WIOC concentration in the Denali core is thus significantly lower than in ice cores from the Alps. The WIOC concentrations range from 6 to 31 $\mu g\,C\,kg^{-1}$ ice with an average of $13 \pm 7\,\mu g\,C\,kg^{-1}$ (Table 1). This is slightly higher than in snow at Summit, Greenland ($4.6\,\mu g\,C\,kg^{-1}$; Hagler et al., 2007), but only about half of the pre-industrial WIOC concentrations in European Alpine ice cores, with $24 \pm 9\,\mu g\,C\,kg^{-1}$ (Legrand et al., 2007) and $32 \pm 18\,\mu g\,C\,kg^{-1}$ (Jenk et al., 2009) from Colle Gnifetti, Monte Rosa, Switzerland, and $24 \pm 7\,\mu g\,C\,kg^{-1}$ from Fiescherhorn Glacier (Jenk et al., 2006). In agreement with findings from previous studies (Legrand et al., 2007), the concentration of DOC ($80\,\mu g\,C\,kg^{-1}$), measured in the deepest sample, was significantly higher than the concentration of WIOC.

The ^{14}C calibration was performed using the OxCal in-built sequence model (Ramsey, 2008, 2017; see Methods). The assumption that samples are in chronological order allows statistical constraints for the most likely age distribu-

tion of the individual samples in the sequence. This assumption of chronological ordering will be discussed below. Samples containing less than 10 µg C are generally characterized by a wide range of age probability. A reduction in the dating precision for those samples is expected due to the small carbon amount available for analysis. Small amounts on the one hand cause reduced AMS measurement precision (lower ^{12}C current and fewer ^{14}C counts) and a lower, unfavorable signal-to-noise ratio (i.e., the ratio between size of sample and procedural blank) on the other hand. Combined, this leads to a larger overall analytical uncertainty, finally translating into a wider range of possible ages. Although we used a considerable amount of ice for each sample ($\sim$ 1 kg), the total carbon amount in five samples was significantly below this 10 µg C threshold recommended to obtain a reliable dating with a final uncertainty < 20 % for samples older than around 1000 years (Uglietti et al., 2016). These samples will thus not be discussed in the following (but can be found in the Supplement, together with calibration results without sequence constraints).

Calibrated ^{14}C ages range from 0.3 ± 0.3 ka cal BP at 166.2 m (131.4 m w.e.) depth to 8.4 ± 0.6 ka cal BP for the deepest sample (Denali235; 209.1 m or 169.8 m w.e.), the last sample above bedrock (0.6 m). These results show the characteristic exponential increase in age with depth, expected for a cold glacier archive due to the associated ice flow dynamics (e.g., Dansgaard and Johnsen, 1969; see also Sect. 4.1.), and most importantly, reveal ice of early Holocene origin in the Denali ice core (Table 1 and Fig. 3). The absolute ages from radiocarbon dating are in agreement with the independently derived ages from the ALC reported in Winski et al. (2017), extended back to 339 CE in this study (see Sect. 3.2 "Annual layer counting"). For the youngest sample, Denali183 from a depth of 166.2 m (131.4 m w.e.), and for Denali214 from 192.6 m (155.0 m w.e.), the 1σ age range is 4–679 and 958–1410 yr cal BP, respectively – similar to the corresponding ALC-derived ages of 340–380 and 1200–1410 yr BP. The 1σ ^{14}C age range for Denali210-211 at 189.5 m (152.3 m w.e.) is 527–930 yr cal BP and with a possible age of 930 yr cal BP only slightly younger than the ALC-derived age range of 1020–1200 yr BP (in agreement within the 2σ range of 317–1174 yr cal BP).

Samples of indistinguishable ages, with regard to the dating uncertainty achieved (i.e., analytical precision), were observed in the depth interval from 200.3 to 206.2 m (161.9 to 167.2 m w.e.). This interval corresponds to a time period from around 3.2 to 4.3 kyr BP. For the respective samples (Denali223, Denali224-225, Denali229-230, Denali231), a low agreement index (denoted as A in OxCal) resulted for the applied ^{14}C calibration approach. A indicates the level of agreement between the probability function derived by the ordinary calibration approach (a priori distribution) and the calibration with an additional constraint (a posterior distribution; see OxCal and Ramsey, 2008, 2017, for more details). Distributions are shown in Fig. 3. A value of 100 indicates no
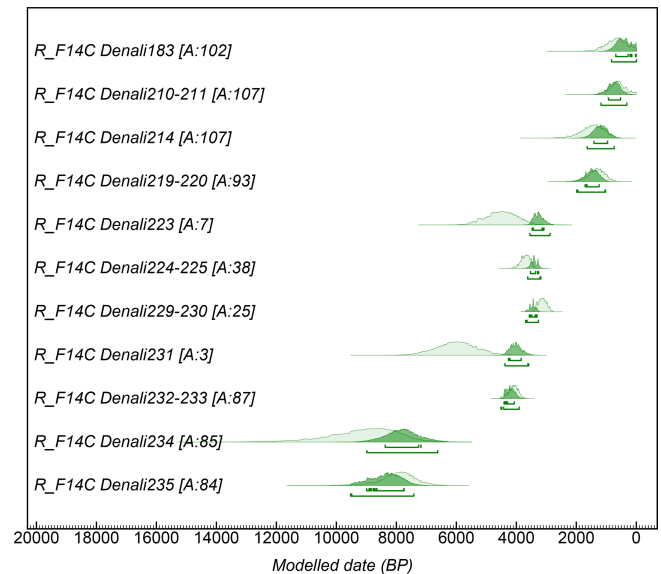

Figure 3. Calibrated ^{14}C age probability distributions for samples from the Denali ice core (DEN-13B), as derived in OxCal v4.4.4 using the IntCal 20 radiocarbon calibration curve (Ramsey, 2021; Reimer et al., 2020). Light green areas indicate the a priori age probabilities and the dark green areas the a posteriori probabilities when sequential ordering of samples is assumed (see main text). The agreement index (A) indicates overlap between these two probability functions. A value < 60 indicates poor agreement (see main text). The 1σ and 2σ range is indicated by the lines below the probability distribution areas.

alteration in the distribution (100 % or unity), while a value lower than 60 indicates a warning to check for the validity of the underlying assumption, i.e., (i) a non-sequential layering of samples or (ii) the presence of analytical outliers. It is apparent from Fig. 3 that the two samples with lowest A (< 10), Denali223 and Denali231, are also characterized by an exceptionally large uncertainty. For the batch of samples with AMS lab IDs BE-10013.1.1 to BE-10022.1.1 (Table 1; see also Supplement Fig. S1 and Table S1), the contribution to the final overall uncertainty from AMS analysis alone was around twice as much as what typically can be achieved for samples of that carbon mass. For that measurement day, we also observed above-average uncertainties for the measured sets of AMS calibration standards, with a slight elevation in the fossil standard value (+0.02 in F^{14}C; see Methods). This is an indication of non-ideal AMS conditions due to sub-optimal instrument tuning on the one hand and an elevated, potentially non-stable background that day on the other hand. Thus, neither ^{14}C ages nor the englacial stratigraphy gives sufficient evidence to conclude a non-sequential ordering of samples (i.e., an age reversal in the Denali ice core). Additionally, there is evidence from other studies from the region suggesting hydrological changes between around 4 to 2 kyr BP (e.g., increased lake levels and precipitation; see Discussion), which coincides with the time period in ques-

tion here. Because increased accumulation rates would lead to a reduced increase in age per unit depth, an unambiguous resolving of the sequence then depends on the achievable analytical uncertainty. Having pushed the limit of the analytical method with the small amounts of carbon available for ^{14}C analysis and considering all the above, we thus exclude assumption (i) and are confident that the applied ^{14}C sequence calibration approach does provide us with the most accurate dates.

4 Discussion

4.1 Denali ice core chronology

Modeling the age scale in high-elevation mountain ice cores can be attempted either by applying rather simple glaciological one-dimensional (1D) flow models (e.g., Nye, 1963; Dansgaard and Johnsen, 1969; Bolzan, 1985) or by much more complex three-dimensional (3D) models based on a suite of observational data from the glaciological survey (e.g., Campbell et al., 2013; Licciulli et al., 2020). Independent of model complexity, age scale modeling, particularly of mountain glaciers, is strongly challenged to provide accurate or even conclusive ages along the profile at a specific point on the glacier (e.g., the ice core drill site; Campbell et al., 2013; Licciulli et al., 2020). This is especially the case close to bedrock, where ice flow can become highly complex and because past annual net accumulation rates with potential variations over time are unknown. Layers of known age along a glacier depth profile, e.g., from ice core dating, can provide crucial model constraints, allowing free model parameters to be tuned for a best fit between observations and model output. For a defined point, moving along a single axis (bed to surface), 1D models benefit from their simplicity to do so (less parameters). 1D models have been applied for decades to obtain continuous age–depth relationships at sites on polar ice sheets (e.g., Dansgaard and Johnsen, 1969), thereby also accounting for past changes in accumulation rates by inverse modeling approaches (e.g., Buiron et al., 2011; Buchardt and Dahl-Jensen, 2008). However, applications to sites from high-mountain glaciers are more recent (e.g., Jenk et al., 2009; Uglietti et al., 2016).

In the case of the Denali ice core, accurate dating by ALC supported with independent time horizons for the upper two-thirds of the core and absolute-dated horizons for the deep section of the core (^{14}C dates) is available. Winski et al. (2017) developed a well-defined age scale for the upper part of the core based on ALC supported by distinct time horizons. Since age–depth relationships are less challenging to model in the upper 90 % of the ice core, because of relatively moderate layer thinning and little if any influence from bedrock, Winski et al. (2017) used a combination of 1D modeling and a 3D glacier flow model developed for this site (Campbell et al., 2013) to determine a significant increase in

accumulation rates since around 1850 CE. Therefore, significant changes in net accumulation rates at the Denali ice core drill site should be expected to a have also occurred in the more distant past.

Due to its simplicity, we used the 1D two-parameter model (2p-model; Bolzan, 1985) to provide a first, best estimate for a continuous age–depth relationship from surface to bedrock, building on the available data points presented. The 2p-model is based on a simple analytical expression for the decrease in the annual layer thickness with depth and has 2 degrees of freedom, the mean annual net accumulation rate b and the thinning parameter p, characterizing the strain rate function; both are assumed to be constant over time. Knowing the glacier thickness of 209.7 m from the ice core length (supported by ground-penetrating radar data; 170.4 m w.e.) and with all depths converted from meters to meters water equivalent based on the ice core density profile allowed us to find the best solutions for b and p by fitting the model (least squares approach, as described in Fahnestock et al., 2001) through the time horizons in the Denali ice core (volcanos, ^{137}Cs, ^{14}C). The derived value for p was 0.79 ± 0.01. The resulting value of b of 1.5 ± 0.1 m w.e. yr^{-1}, representing the mean annual net accumulation rate for the entire period covered by the ice core, is similar to the recently observed 21st century values. It is however significantly higher than the average value of around 0.5 m w.e. yr^{-1} previously determined for the last 810 years (ranging from around 0.3 to 1.5 m w.e. yr^{-1}; Winski et al., 2017). This is no surprise, considering the likelihood that similar variations may also have occurred further back in time. As a consequence of being constrained by the age of dated layers, the model results are in agreement with the observational data for the total time period covered within the ice column. However, at various depths along the depth profile, a significant offset between model output and data can be observed (Fig. 4a). Again, this is not unexpected considering the fact that the accumulation rate was kept constant in the model, while significant changes over time are known to have occurred (Winski et al., 2017). In Fig. 3a, the effect on model results for variations in b is illustrated (runs with b equal to 0.5, 1.5, and 2 m w.e. yr^{-1}, with p determined as before).

To achieve our final goal, obtaining a continuous age–depth relationship based on the absolute dating presented, we next applied a simple inverse modeling approach. We tightly fit the model to the experimental data by numerically solving for the exact value of b for each depth with a determined age (p and H as before). To reduce and account for potential noise in the data, an uncertainty-weighted three-point running mean to obtain the non-steady-state values for b was calculated (starting from top, then reversed from bottom, thereby propagating the values for continuity). These values, interpolated for depths between the dated layers, were finally used for model input, yielding a continuous age–depth relationship (Fig. 4b and c). All uncertainties have been fully propagated throughout the calculations
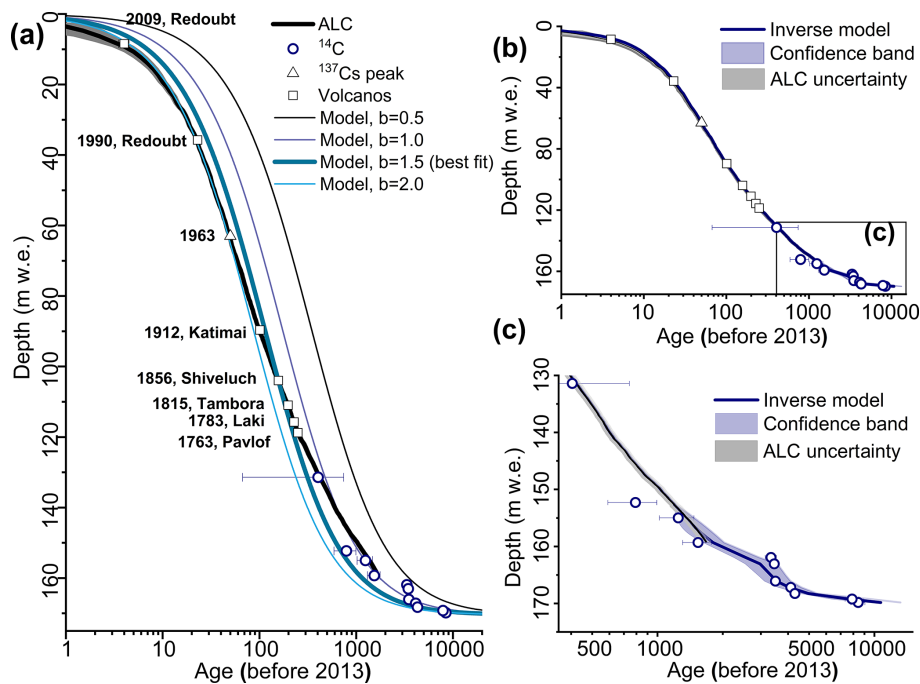
Figure 4. Denali ice core (DEN-13B): annual layer counting (ALC), dating horizons (^{14}C, volcanos, ^{137}Cs peak), and modeled, continuous age–depth relationship (1D ice flow model; see main text). **(a)** Model output for constant accumulation rates (b, in m w.e. yr^{-1}). **(b)** Modeled age–depth relationship for variable b (inverse model). **(c)** Zoom of the deepest part. All error bars indicate the 1σ uncertainty.

(from analysis to modeling). We derived annual net accumulation rates of 0.5 ± 0.1 m w.e. yr^{-1} at around 1000 CE, eventually increasing to a 20th century average value of 1.1 ± 0.2 m w.e. yr^{-1} (Fig. S2). This is in good agreement with what was determined previously by Winski et al. (2017) for the corresponding periods, based on results from different models investigated (for the 3D model considered best, 0.25 m w.e. yr^{-1} around 1000 CE, with models ranging from 0.05–0.7 m w.e. yr^{-1}, and 1.1 ± 0.3 m w.e. yr^{-1} for the 20th century average). During the Holocene Climate Optimum (around 8 to 5 kyr BP, Kaufman et al., 2016) we obtained net accumulation rates of 1.2 ± 0.3 m w.e. yr^{-1}, similar to the average rate observed since 1950 CE, followed by higher rates of 1.7 ± 0.4 m w.e. yr^{-1} from around 4.3 to 3.2 kyr BP. Then, the rates decrease over the next 500 to 1000 years to around 0.4 ± 0.2 m w.e. yr^{-1}. See Sect. 4.3 for further discussion. Our derived age–depth scale results in ages of 9–14 kyr BP at 0.5 m above bedrock, strongly suggesting the presence of at least early Holocene ice at the Denali ice core drill site.

4.2 Ice core chronologies in Eastern Beringia

So far, existing ice cores from Eastern Beringia (Table 2) were dated with ages covering less than the last millennium except for the Denali core discussed in this study and the 188 m long PRCol core (Fig. 1) drilled to the bed surface on the summit plateau of Mt. Logan in 2001 and 2002. The older part of the PRCol core was dated based on a signal inter-

preted as the Younger Dryas to Holocene transition (sudden reduction in electrical conductivity coinciding with a drop in δ^{18}O and an increase in various chemical species) and a bottom age estimate from an ice flow model of about 20 ka (Fisher et al., 2008). Another ice core from Mt. Logan (King Col; 60.59° N, 140.60° W; 4135 m a.s.l.) was drilled in 2002 reaching a depth of 220.5 m. This core was not dated, but a potential age range of 0.5 to 1.3 ka was estimated based on modeling results (Shiraiwa et al., 2003). The 152 m ice core drilled in 2008 on the McCall Glacier was dated by using a combination of ALC and specific horizons. The upper 37 m of ice date back to 65 years, and the full 152 m core was estimated to cover more than 200 years, but no actual dating of the lower section was performed (Klein et al., 2016). The Aurora Peak site is located southeast of Mt. Hayes, and the ice core was also drilled in 2008. The total ice thickness at the drilling site is 252 ± 10 m, but this core (180.17 m) did not approach the bed surface. By annual layer counting, the estimated bottom age of the Aurora Peak core is about 274 years (Tsushima et al., 2015). Two cores were collected at Eclipse Icefield in 2002. The chronology of these cores is based on multi-parameter ALC of seasonal oscillations in the stable isotope (δ^{18}O) and major ion records (Na$^+$) supported by the identification of volcanic horizons. The longest core (345 m) covers the period 1000 to 2002 CE (Yalcin et al., 2007) but did not reach bedrock. In 2004, a 212 m ice core was drilled from Mt. Wrangell. The ice depth in the summit caldera is probably over 900 m, but the definite bottom has not yet been

Table 2. Overview of existing North Pacific ice cores.

Site	Year of drilling (CE)	Latitude (° N)	Longitude (° W)	Elevation (m a.s.l.)	Depth (m)	Reported time span (yr)
McCall Glacier[a]	2008	69.17	143.47	2310	152	> 200
Aurora Peak[b]	2008	63.52	146.54	2825	180	274
Begguya[c]	2013	62.56	151.05	3900	208	> 8000
Mt. Wrangell[d]	2004	62.00	144.00	4317	212	23
Bona-Churchill[e]	2002	61.40	141.42	4420	461	∼ 800
Mt. Logan PRCol[f]	2001–2002	60.59	140.50	5340	188	∼ 20 000
Eclipse Icefield[g]	2002	60.51	139.47	3017	345	∼ 1000
Mt. Waddington[h]	2010	51.38	125.26	3000	141	∼ 40

[a] McCall Glacier (Klein et al., 2016). [b] Aurora Peak (Tsushima, 2015). [c] Begguya (this study). [d] Mt. Wrangell (Yasunari et al., 2007; Sasaki et al., 2016). [e] Bona-Churchill (Porter et al., 2019). [f] Mt. Logan (Fisher et al., 2008). [g] Eclipse Icefield (Yalcin et al., 2007). [h] Mt. Waddington (Neff et al., 2012).

detected (Benson et al., 2007). For this core, a short 12-year record of dust and δD was reported in Yasunari et al. (2007), and dating was later extended back to 1981 (23 years) at the depth of 100.1 m (Sasaki et al., 2016). The record from Mt. Waddington only covers a period of 1973–2010 CE (Neff et al., 2012). The total length of the Mt. Waddington core is 141 m, but the total ice thickness at the drilling site is about 250 m. The ice core from Bona-Churchill reached bedrock at a depth of 460 m, but the age–depth scale has only been established for the last ∼ 800 years (depth of 399 m); the deepest ice is estimated to exceed 1500 years in age (Porter et al., 2019).

Because none of the cores from the Eastern Beringia region was drilled to the bed surface and no ice close to the bed was ever dated by an absolute dating method, no conclusive evidence about the age of the oldest glacier ice preserved in this region exists so far. In this study, we achieved a first complete and absolute (radiometric) dating through the first application of ^{14}C analysis on a high-latitude Northern Hemisphere ice core from Begguya, which reached the bed surface. Our results, with calibrated ^{14}C ages of 7.7 to 9.0 kyr BP close to the bottom (0.61 m above bedrock) and model-based indication for potentially even older ice further below (> 12 kyr BP), clearly indicate that glaciers in this region can be of early Holocene or even Pleistocene origin.

4.3 Possible implications for Holocene hydroclimate in Eastern Beringia

In recent decades, extensive work has been done in the North Pacific region to characterize Holocene hydroclimate (Table 3, Fig. 5). Following a modest Holocene thermal maximum that was 0.2–0.5 °C warmer than the last millennium average (Kaufman et al., 2016), although 1.7 °C cooler than present (Porter et al., 2019), glaciers across the region advanced synchronously at about 4.5 kyr BP (Solomina et al., 2015). This Neoglaciation continued through 3.5 to 2.5 kyr BP in the Yukon Territory based on past tree line
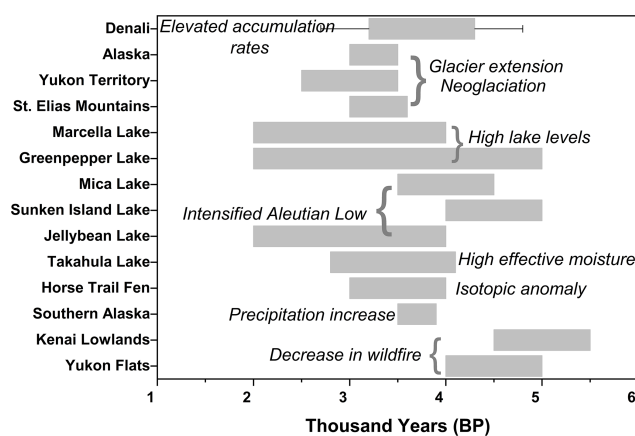

Figure 5. Regional paleoclimate changes as reported in previous studies (Anderson et al., 2005a, b, 2006, 2016, 2019; Broadman et al., 2020; Clegg and Hu, 2010; Denton and Karlén, 1977; Heusser et al., 1985; Jones et al., 2019; Kelly et al., 2013; Schiff et al., 2009; Solomina et al., 2015) and the period of elevated annual net accumulation rates indicated in the Denali ice core DEN-13B (this study; see main text).

variations, lake levels, and carbonate oxygen isotopes (Denton and Karlén, 1977; Anderson et al., 2005a). While a mid-Holocene temperature decrease may have played a role, Denton and Karlen (1977) hypothesized that an increase in regional precipitation contributed to the regional Neoglaciation, a conclusion also reached by later studies (e.g., Anderson et al., 2011).

Concurrent with this Neoglaciation, effective moisture rose across much of the region. Based on pollen reconstructions, Heusser et al. (1985) inferred a doubling of southern Alaskan mean annual precipitation from around 3.9 to 3.5 kyr BP (Fig. 3). Clegg and Hu (2010) found that effective moisture, particularly during winters, increased markedly between 4.0 and 2.5 kyr BP. Hansen and Engstrom (1996) suggested cooler and wetter conditions in Glacier Bay at around

Table 3. Regional paleoclimate events.

Location	Reference	Paleoclimate events	Time (kyr BP)
Begguya	This study	Elevated net accumulation rates	4.3 ± 0.5 to 3.2 ± 0.5
Yukon Territory	Denton and Karlén (1977); Anderson et al. (2005b)	Neoglaciation	3.5 to 2.5
St. Elias Mountains	Denton and Karlén (1977)	Glacier extension	3.6 to 3.0
Alaska	Solomina et al. (2015)	Glacier extension	3.5 to 3.0
Marcella Lake	Anderson et al. (2005b)	High lake levels	4.0 to 2.0
Greenpepper Lake	Anderson et al. (2019)	High lake levels	5.0 to 2.0
Jellybean Lake	Anderson et al. (2005a)	Intensified Aleutian Low	4.0 to 2.0
Mica Lake	Schiff et al. (2009)	Intensified Aleutian Low	4.0 ± 0.5
Sunken Island Lake	Broadman et al. (2020)	Intensified Aleutian Low	5.0 to 4.0
Takahula Lake	Clegg and Hu (2010)	High effective moisture	4.0 to 2.5
Horse Trail Fen	Jones et al. (2019)	Isotopic anomaly	4.0 to 3.0
Southern Alaskan	Heusser et al. (1985)	Precipitation increases	3.9 to 3.5
Kenai Lowlands	Anderson et al. (2006)	Decrease in wildfire	5.5 to 4.5
Yukon Flats	Kelly et al. (2013)	Decrease in wildfire	5.0 to 4.0

3.4 kyr BP. At Jellybean Lake and Marcella Lake, lake levels were high between 2.0–4.0 kyr BP (Anderson et al., 2005a, b), which was attributed to changes in the strength and positions of the Aleutian Low (Anderson et al., 2005b), consistent with the more recent interpretation of hydroclimate changes from the Denali ice core (Winski et al., 2017; Osterberg et al., 2017). Records from Mica Lake (Schiff et al., 2009) and Sunken Island Lake (Broadman et al., 2020) showed wetter conditions associated with a stronger Aleutian Low at 4 kyr and 4.5 kyr BP, respectively. Greenpepper Lake experienced high lake levels from 2–5 kyr BP (Anderson et al., 2019), and a major shift from moss to sedge occurred at Horse Trail Fen, concurrent with a large isotopic anomaly at 3–4 kyr BP (Jones et al., 2019). At the same time, paleoenvironmental records showed a decrease in wildfire (Anderson et al., 2006; Kelly et al., 2013).

Together, previous work indicates an enhanced flux of moisture into the region, likely associated with a strengthened Aleutian Low, sometime near 4 kyr BP (Anderson et al., 2016). The Denali ice core may provide corroborating evidence for this mid-Holocene shift in hydroclimate (Table 3, Fig. 5). As presented before, samples of indistinguishable ages, at least for the achieved analytical precision, were observed in the depth interval from 200.3 to 206.2 m (161.9–167.2 m w.e.), corresponding to the modeled time period from 4.3 ± 0.5 to 3.2 ± 0.5 kyr BP (see Sects. 3.3 "Denali ice core ^{14}C data" and 4.1 "Denali ice core chronology"). Elevated snow accumulation provides a possible explanation for this clustering of dates and would support many previous studies. While our model results based on ^{14}C ages are consistent with existing interpretations of mid-Holocene changes in regional precipitation, applying other independent dating methods using the remaining parallel ice sections from this depth interval (e.g., from DEN-13B) could be used, and ad-

ditional geophysical and modeling approaches are needed to rigorously test this hypothesis.

Importantly, some hydroclimate studies do not show a shift toward wetter conditions at 4 kyr BP. On Adak Island, conditions grew cooler and drier at 4.5 kyr BP, which is consistent with the prevailing interpretation of a stronger Aleutian Low advecting warmer, moister air into the Gulf of Alaska and cooler, drier air to the western Aleutians (Bailey et al., 2018). Certain sites located to the north of the Alaska or St. Elias ranges also show a drying trend or no major features around 4 kyr BP (Lasher et al., 2021; Finney et al., 2012; King et al., 2022; Chakraborty et al., 2010), emphasizing the idea that orography and rain shadows are critical for controlling the relationship between site precipitation and circulation (Anderson et al., 2016). In fact, Winski et al. (2017) showed that during the instrumental era, Begguya snowfall is highly correlated with precipitation along the Gulf of Alaska but bears little resemblance to nearby precipitation recorded in interior Alaska – a pattern that seems to hold through the mid-Holocene. We note that the Aleutian Low is a wintertime phenomenon such that the role of summertime precipitation may be an important contributor to some of the observed variability among regional paleorecords. Comparing records with different seasonality or with seasonal resolution will be critical in the future given that most of the isotope-based records listed above are dominated by wintertime Aleutian Low dynamics.

5 Conclusions

Although ^{14}C analysis of ice-incorporated carbonaceous aerosols has allowed radiocarbon dating of various high-elevation ice cores from low and midlatitudes, this technique has not been applied before for high-latitude ice cores because of the generally lower carbon content. The ^{14}C results

from the Denali ice core are the first from a high-latitude ice core. These were achieved by small adaptations in the ice sample preparation procedures for the WIOC ^{14}C dating method which allowed the processing of larger ice samples up to > 1 kg of ice and the application of a new technique for ^{14}C dating of the DOC fraction, which benefits from higher concentration levels in ice compared to the WIOC fraction (by around a factor of 3). Combining dating by ALC to a depth of 197.2 m (159.2 m w.e.; ∼ 1674 years BP or 339 CE); volcanic tie points from sulfate, chloride, and conductivity; and the new ^{14}C-dated horizons, a complete continuous chronology over the entire core was established using a simple inverse ice flow modeling approach. For the overlapping sections, ages based on ALC are confirmed by the agreement with the absolute, radiometric ^{14}C dates.

The ^{14}C dating of a sample from just 0.61 m above bedrock at around 209 m depth yielded the first absolute date for near-bedrock ice in the region. Dated to be 7700 to 9000 years old, our result clearly indicates this ice at the very bottom is of early Holocene age. The additional model results indicate a high likelihood of even older ice below (> 12 ka). The old ice at the bottom of the Denali core confirms that at least some glacier ice in the central Alaska Range survived the Holocene thermal maximum. Future, independent dating methods would be beneficial to further constrain and improve the timescale presented here. Our results show the applicability and great potential of ^{14}C dating on low-carbon-content samples from North Pacific and Arctic ice cores. While they indicate the Denali ice core is currently one of the few existing archives in the North Pacific region providing an opportunity to reconstruct Holocene hydroclimate variability, we do expect that similar or even longer paleo-ice-core records can be recovered from North Pacific glaciers if bedrock can be reached.

Author contributions. LF, TMJ, and MS performed ^{14}C analysis, evaluation, and the continuous age–depth scale modeling. DW, KK, EO, SC, HLB, and CW drilled the core and/or conducted the chemical and physical property analysis. HLB, DW, and EO identified the annual layers. EE provided the radar image. LF, TMJ, DW, KK, and MS wrote the manuscript, and all authors contributed to the discussion of the results.

References

Agrios, K., Salazar, G., Zhang, Y. L., Uglietti, C., Battaglia, M., Luginbühl, M., Ciobanu, V. G., Vonwiller, M., and Szidat, S.: Online coupling of pure O_2 thermo-optical methods–^{14}C AMS for source apportionment of carbonaceous aerosols, Nucl. Instrum. Methods, 361, 288–293, 2015.

Agrios, K., Salazar, G., and Szidat, S.: A Continuous-Flow Gas Interface of a Thermal/Optical Analyzer With ^{14}C AMS for Source Apportionment of Atmospheric Aerosols, Radiocarbon, 59, 921–932, 2017.

Anderson, L., Abbott, M. B., Finney, B. P., and Edwards, M. E.: Palaeohydrology of the Southwest Yukon Territory, Canada, based on multiproxy analyses of lake sediment cores from a depth transect, Holocene, 15, 1172–1183, 2005a.

Anderson, L., Abbott, M. B., Finney, B. P., and Burns, S. J.: Regional atmospheric circulation change in the North Pacific during the Holocene inferred from lacustrine carbonate oxygen isotopes, Yukon Territory, Canada, Quaternary Res., 64, 21–35, 2005b.

Anderson, L., Finney, B. P., and Shapley, M. D.: Lake carbonate-δ^{18}O records from the Yukon Territory, Canada: Little Ice Age moisture variability and patterns, Quaternary Sci. Rev., 30, 887–898, 2011.

Anderson, L., Berkelhammer, M., Barron, J. A., Steinman, B. A., Finney, B. P., and Abbott, M. B.: Lake oxygen isotopes as

recorders of North American Rocky Mountain hydroclimate: Holocene patterns and variability at multi-decadal to millennial time scales, Global Planet. Change, 137, 131–148, 2016.

Anderson, L., Edwards, M., Shapley, M. D., Finney, B. P., and Langdon, C.: Holocene thermokarst lake dynamics in northern interior Alaska: the interplay of climate, fire, and subsurface hydrology, Front. Earth Sci., 7, 53, https://doi.org/10.3389/feart.2019.00053, 2019.

Anderson, R. S., Hallett, D. J., Berg, E., Jass, R. B., Toney, J. L., de Fontaine, C. S., and DeVolder, A.: Holocene development of boreal forests and fire regimes on the Kenai Lowlands of Alaska, Holocene, 16, 791–803, 2006.

Bailey, H. L., Kaufman, D. S., Sloane, H. J., Hubbard, A. L., Henderson, A. C., Leng, M. J., Meyer, H., and Welker, J. M.: Holocene atmospheric circulation in the central North Pacific: A new terrestrial diatom and $\delta^{18}O$ dataset from the Aleutian Islands, Quaternary Sci. Rev., 194, 27–38, 2018.

Barclay, D. J., Wiles, G. C., and Calkin, P. E.: Holocene glacier fluctuations in Alaska, Quaternary Sci. Rev., 28, 2034–2048, 2009.

Bengtsson, L., Semenov, V. A., and Johannessen, O. M.: The Early Twentieth-Century Warming in the Arctic-A Possible Mechanism, J. Climate, 17, 4045–4057, https://doi.org/10.1175/1520-0442(2004)017<4045:tetwit>2.0.co;2, 2004.

Benson, C., Motyka R., Mcnutt, S., Luethi, M., and Truffer, M.: Glacier–volcano interactions in the North Crater of Mt Wrangell, Alaska, Ann. Glaciol., 45, 48–57, 2007.

Blackport, R., Screen, J. A., van der Wiel, K., and Bintanja, R.: Minimal influence of reduced Arctic sea ice on coincident cold winters in mid-latitudes, Nat. Clim. Change, 9, 697–704, 2019.

Bolzan, J. F.: Ice flow at the Dome C ice divide based on a deep temperature profile, J. Geophys. Res.-Atmos., 90, 8111–8124, 1985.

Brennan, P. V., Lok, L. B., Nicholls, K., and Corr, H.: Phase-sensitive FMCW radar system for high-precision Antarctic ice shelf profile monitoring, IET Radar Sonar Nav., 8, 776–786, 2014.

Broadman, E., Kaufman, D. S., Henderson, A. C., Berg, E. E., Anderson, R. S., Leng, M. J., Stahnke, S. A., and Muñoz, S. E.: Multi-proxy evidence for millennial-scale changes in North Pacific Holocene hydroclimate from the Kenai Peninsula lowlands, south-central Alaska, Quaternary Sci. Rev., 241, 106420, https://doi.org/10.1016/j.quascirev.2020.106420, 2020.

Buchardt, S. L. and Dahl-Jensen, D.: At what depth is the Eemian layer expected to be found at NEEM?, Ann. Glaciol., 48, 100–102, 2008.

Buiron, D., Chappellaz, J., Stenni, B., Frezzotti, M., Baumgartner, M., Capron, E., Landais, A., Lemieux-Dudon, B., Masson-Delmotte, V., Montagnat, M., Parrenin, F., and Schilt, A.: TALDICE-1 age scale of the Talos Dome deep ice core, East Antarctica, Clim. Past, 7, 1–16, https://doi.org/10.5194/cp-7-1-2011, 2011.

Campbell, S., Roy, S., Kreutz, K., Arcone, S. A., Osterberg, E. C., and Koons, P.: Strain-rate estimates for crevasse formation at an alpine ice divide: Mount Hunter, Alaska, Ann. Glaciol., 54, 200–208, 2013.

Chakraborty, K., Finkelstein, S. A., Desloges, J. R., and Chow, N. A.: Holocene paleoenvironmental changes inferred from diatom assemblages in sediments of Kusawa Lake, Yukon Territory, Canada, Quaternary Res., 74, 15–22, 2010.

Choi, Y., Rhee, T. S., Collett Jr, J. L., Park, T., Park, S.-M., Seo, B.-K., Park, G., Park, K., and Lee, T.: Aerosol concentrations and composition in the North Pacific marine boundary layer, Atmos. Environ., 171, 165–172, 2017.

Clegg, B. F. and Hu, F. S.: An oxygen-isotope record of Holocene climate change in the south-central Brooks Range, Alaska, Quaternary Sci. Rev., 29, 928–939, 2010.

Cohen, J., Screen, J. A., Furtado, J. C., Barlow, M., Whittleston, D., Coumou, D., Francis, J., Dethloff, K., Entekhabi, D., and Overland, J.: Recent Arctic amplification and extreme mid-latitude weather, Nat. Geosci., 7, 627–637, 2014.

Cohen, J., Pfeiffer, K., and Francis, J. A.: Warm Arctic episodes linked with increased frequency of extreme winter weather in the United States, Nat. Commun., 9, 869, https://doi.org/10.1038/s41467-018-02992-9, 2018.

Cohen, J., Zhang, X., Francis, J., Jung, T., Kwok, R., Overland, J., Ballinger, T., Bhatt, U., Chen, H., and Coumou, D.: Divergent consensuses on Arctic amplification influence on mid-latitude severe winter weather, Nat. Clim. Change, 10, 20–29, https://doi.org/10.1038/s41558-019-0662-y, 2019.

Dansgaard, W. and Johnsen, S.: A flow model and a time scale for the ice core from Camp Century, Greenland, J. Glaciol., 8, 215–223, 1969.

Denton, G. H. and Karlén, W.: Holocene glacial and tree-line variations in the White River Valley and Skolai Pass, Alaska and Yukon Territory, Quaternary Res., 7, 63–111, 1977.

Dorch, J. M.: Defining the Timing of Glaciation in the Central Alaska Range, Doctoral dissertation, University of Cincinnati, 2007.

Fahnestock, M., Abdalati, W., Luo, S., and Gogineni, S., Internal layer tracing and age-depth-accumulation relationships for the northern Greenland ice sheet, J. Geophys. Res.-Atmos., 106, 33789–33797, 2001.

Fang, L., Schindler, J., Jenk, T. M., Uglietti, C., Szidat, S., and Schwikowski, M.: Extraction of Dissolved Organic Carbon from Glacier Ice for Radiocarbon Analysis, Radiocarbon, 61, 681–694, 2019.

Fang, L., Jenk, T. M., Singer, T., Hou, S., and Schwikowski, M.: Radiocarbon dating of alpine ice cores with the dissolved organic carbon (DOC) fraction, The Cryosphere, 15, 1537–1550, https://doi.org/10.5194/tc-15-1537-2021, 2021.

Finney, B. P., Bigelow, N. H., Barber, V. A., and Edwards, M. E.: Holocene climate change and carbon cycling in a groundwater-fed, boreal forest lake: Dune Lake, Alaska, J. Paleolimnol., 48, 43–54, 2012.

Fisher, D., Osterberg, E., Dyke, A., Dahl-Jensen, D., Demuth, M., Zdanowicz, C., Bourgeois, J., Koerner, R. M., Mayewski, P., and Wake, C.: The Mt Logan Holocene–late Wisconsinan isotope record: tropical Pacific–Yukon connections, Holocene, 18, 667–677, 2008.

Francis, J. A., Vavrus, S. J., and Cohen, J.: Amplified Arctic warming and mid-latitude weather: new perspectives on emerging connections, Wiley Interdiscip. Rev. Clim. Change, 8, e474, https://doi.org/10.1002/wcc.474, 2017.

Godwin, H.: Half-life of radiocarbon, Nature, 195, 984, 1962.

Hagler, G. S., Bergin, M. H., Smith, E. A., Dibb, J. E., Anderson, C., and Steig, E. J.: Particulate and water-soluble carbon measured in recent snow at Summit, Greenland, Geophys. Res. Lett., 34, L16505, https://doi.org/10.1029/2007GL030110, 2007.

Hansen, B. C. and Engstrom, D. R.: Vegetation history of Pleasant Island, southeastern Alaska, since 13,000 yr BP, Quaternary Res., 46, 161–175, 1996.

Haque, M. M., Kawamura, K., and Kim, Y.: Seasonal variations of biogenic secondary organic aerosol tracers in ambient aerosols from Alaska, Atmos. Environ., 130, 95–104, 2016.

Heusser, C. J., Heusser, L., and Peteet, D.: Late-Quaternary climatic change on the American North Pacific coast, Nature, 315, 485–487, 1985.

Hoffman, H. M.: Micro radiocarbon dating of the particulate organic carbon fraction in Alpine glaicer ice: method refinement, critical evaluation and dating applications, DhD thesis, Ruperto-Carola University of Heidelberg, https://doi.org/10.11588/heidok.00020712, 2016.

Hou, S., Jenk, T. M., Zhang, W., Wang, C., Wu, S., Wang, Y., Pang, H., and Schwikowski, M.: Age ranges of the Tibetan ice cores with emphasis on the Chongce ice cores, western Kunlun Mountains, The Cryosphere, 12, 2341–2348, https://doi.org/10.5194/tc-12-2341-2018, 2018.

Jenk, T. M., Szidat, S., Schwikowski, M., Gäggeler, H. W., Brütsch, S., Wacker, L., Synal, H.-A., and Saurer, M.: Radiocarbon analysis in an Alpine ice core: record of anthropogenic and biogenic contributions to carbonaceous aerosols in the past (1650–1940), Atmos. Chem. Phys., 6, 5381–5390, https://doi.org/10.5194/acp-6-5381-2006, 2006.

Jenk, T. M., Szidat, S., Bolius, D., Sigl, M., Gaeggeler, H. W., Wacker, L., Ruff, M., Barbante, C., Boutron, C. F., and Schwikowski, M.: A novel radiocarbon dating technique applied to an ice core from the Alps indicating late Pleistocene ages, J. Geophys. Res.-Atmos., 114, D14305, https://doi.org/10.1029/2009JD011860, 2009.

Jones, M. C., Anderson, L., Keller, K., Nash, B., Littell, V., Wooller, M., and Jolley, C. A.: An assessment of plant species differences on cellulose oxygen isotopes from two Kenai Peninsula, Alaska peatlands: Implications for hydroclimatic reconstructions, Front. Earth Sci., 7, 25, https://doi.org/10.3389/feart.2019.00025, 2019.

Kaufman, D. S., Axford, Y. L., Henderson, A. C., McKay, N. P., Oswald, W. W., Saenger, C., Anderson, R. S., Bailey, H. L., Clegg, B., and Gajewski, K.: Holocene climate changes in eastern Beringia (NW North America)–A systematic review of multi-proxy evidence, Quaternary Sci. Rev., 147, 312–339, 2016.

Kelly, R., Chipman, M. L., Higuera, P. E., Stefanova, I., Brubaker, L. B., and Hu, F. S.: Recent burning of boreal forests exceeds fire regime limits of the past 10,000 years, P. Natl. Acad. Sci. USA, 110, 13055–13060, 2013.

King, A. L., Anderson, L., Abbott, M., Edwards, M., Finkenbinder, M. S., Finney, B., and Wooller, M. J.: A stable isotope record of late Quaternary hydrologic change in the northwestern Brooks Range, Alaska (eastern Beringia), J. Quaternary Sci., 37, 928–943, 2022.

Klein, E., Nolan, M., McConnell, J., Sigl, M., Cherry, J., Young, J., and Welker, J.: McCall Glacier record of Arctic climate change: Interpreting a northern Alaska ice core with regional water isotopes, Quaternary Sci. Rev., 131, 274–284, 2016.

Lal, D.: Cosmogenic in situ radiocarbon on the earth. Radiocarbon After Four Decades, Springer, 146–161, 1992.

Lal, D. and Jull, A.: On determining ice accumulation rates in the past 40,000 years using in situ cosmogenic ^{14}C, Geophys. Res. Lett., 17, 1303–1306, 1990.

Lal, D., Nishiizumi, K., and Arnold, J.: In situ cosmogenic ^{3}H, ^{14}C, and ^{10}Be for determining the net accumulation and ablation rates of ice sheets, J. Geophys. Res.-Sol. Ea., 92, 4947–4952, 1987.

Lasher, G. E., Abbott, M. B., Anderson, L., Yasarer, L., Rosenmeier, M., and Finney, B. P.: Holocene hydroclimatic reorganizations in northwest Canada inferred from lacustrine carbonate oxygen isotopes, Geophys. Res. Lett., 48, e2021GL092948, https://doi.org/10.1029/2021GL092948, 2021.

Legrand, M., Preunkert, S., Schock, M., Cerqueira, M., Kasper-Giebl, A., Afonso, J., Pio, C., Gelencsér, A., and Dombrowski-Etchevers, I.: Major 20th century changes of carbonaceous aerosol components (EC, WinOC, DOC, HULIS, carboxylic acids, and cellulose) derived from Alpine ice cores, J. Geophys. Res., 112, D23, https://doi.org/10.1029/2006jd008080, 2007.

Legrand, M., Preunkert, S., May, B., Guilhermet, J., Hoffman, H., and Wagenbach, D.: Major 20th century changes of the content and chemical speciation of organic carbon archived in Alpine ice cores: Implications for the long-term change of organic aerosol over Europe, J. Geophys. Res.-Atmos., 118, 3879–3890, 2013.

Licciulli, C., Bohleber, P., Lier, J., Gagliardini, O., Hoelzle, M., and Eisen, O.: A full Stokes ice-flow model to assist the interpretation of millennial-scale ice cores at the high-Alpine drilling site Colle Gnifetti, Swiss/Italian Alps, J. Glaciol., 66, 35–48, 2020.

Lilien, D. A., Hills, B. H., Driscol, J., Jacobel, R., and Christianson, K.: ImpDAR: an open-source impulse radar processor, Ann. Glaciol., 61, 114–123, 2020.

Neff, P. D., Steig, E. J., Clark, D. H., McConnell, J. R., Pettit, E. C., and Menounos, B.: Ice-core net snow accumulation and seasonal snow chemistry at a temperate-glacier site: Mount Waddington, southwest British Columbia, Canada, J. Glaciol., 58, 1165–1175, https://doi.org/10.3189/2012JoG12J078, 2012.

Nye, J.: On the theory of the advance and retreat of glaciers, Geophys. J. Int., 7, 431–456, 1963.

Osterberg, E. C., Mayewski, P. A., Fisher, D. A., Kreutz, K. J., Maasch, K. A., Sneed, S. B., and Kelsey, E.: Mount Logan ice core record of tropical and solar influences on Aleutian Low variability: 500–1998 A.D, J. Geophys. Res.-Atmos., 119, 2014JD021847, https://doi.org/10.1002/2014JD021847, 2014.

Osterberg, E. C., Winski, D. A., Kreutz, K. J., Wake, C. P., Ferris, D. G., Campbell, S., Introne, D., Handley, M., and Birkel, S.: The 1200 year composite ice core record of Aleutian Low intensification, Geophys. Res. Lett., 44, 7447–7454, https://doi.org/10.1002/2017GL073697, 2017.

Park, H.-S., Kim, S.-J., Stewart, A. L., Son, S.-W., and Seo, K.-H.: Mid-Holocene Northern Hemisphere warming driven by Arctic amplification, Sci. Adv., 5, eaax8203, https://doi.org/10.1126/sciadv.aax8203, 2019.

Pendleton, S. L., Ceperley, E. G., Briner, J. P., Kaufman, D. S., and Zimmerman, S.: Rapid and early deglaciation in the central Brooks Range, Arctic Alaska, Geology, 43, 419–422, 2015.

Polashenski, D. J., Osterberg, E. C., Koffman, B. G., Winski, D., Stamieszkin, K., Kreutz, K. J., Wake, C. P., Ferris, D. G., Introne, D., and Campbell, S.: Denali ice core methanesulfonic

acid records North Pacific marine primary production, J. Geophys. Res.-Atmos., 123, 4642–4653, 2018.

Porter, S. E., Mosley-Thompson, E., and Thompson, L. G.: Ice core δ^{18}O record linked to Western Arctic sea ice variability, J. Geophys. Res.-Atmos., 124, 10784–10801, 2019.

Ramsey, C. B.: Deposition models for chronological records, Quaternary Sci. Rev., 27, 42–60, 2008.

Ramsey, C. B.: Methods for summarizing radiocarbon datasets, Radiocarbon, 59, 1809–1833, 2017.

Ramsey, C. B.: OxCal 4.4.4 calibration program, https://c14.arch.ox.ac.uk/oxcal/OxCal.html (last access: 13 July 2023), 2021.

Reimer, P. J., Austin, W. E., Bard, E., Bayliss, A., Blackwell, P. G., Ramsey, C. B., Butzin, M., Cheng, H., Edwards, R. L., and Friedrich, M.: The IntCal20 Northern Hemisphere radiocarbon age calibration curve (0–55 cal kBP), Radiocarbon, 62, 725–757, 2020.

Ruff, M., Wacker, L., Gäggeler, H., Suter, M., Synal, H.-A., and Szidat, S.: A gas ion source for radiocarbon measurements at 200 kV, Radiocarbon, 49, 307–314, 2007.

Sasaki, H., Matoba, S., Shiraiwa, T., and Benson, C.S., Temporal variation in iron flux deposition onto the Northern North Pacific reconstructed from an ice core drilled at Mount Wrangell, Alaska, SOLA, 12, 287–290, https://doi.org/10.2151/sola.2016-056, 2016.

Schiff, C. J., Kaufman, D. S., Wolfe, A. P., Dodd, J., and Sharp, Z.: Late Holocene storm-trajectory changes inferred from the oxygen isotope composition of lake diatoms, south Alaska, J. Paleolimnol., 41, 189–208, 2009.

Screen, J. A. and Francis, J. A.: Contribution of sea-ice loss to Arctic amplification is regulated by Pacific Ocean decadal variability, Nat. Clim. Change, 6, 856–860, https://doi.org/10.1038/nclimate3011, 2016.

Screen, J. A., Deser, C., Smith, D. M., Zhang, X., Blackport, R., Kushner, P. J., Oudar, T., McCusker, K. E., and Sun, L.: Consistency and discrepancy in the atmospheric response to Arctic sea-ice loss across climate models, Nat. Geosci., 11, 155–163, 2018.

Shiraiwa, T., Goto-Azuma, K., Matoba, S., Yamasaki, T., Segawa, T., Kanamori, S., Matsuoka, K., and Fujii, Y.: Ice core drilling at King Col, Mount Logan 2002, B. Glaciol. Res., 20, 57–63, 2003.

Solomina, O. N., Bradley, R. S., Hodgson, D. A., Ivy-Ochs, S., Jomelli, V., Mackintosh, A. N., Nesje, A., Owen, L. A., Wanner, H., and Wiles, G. C.: Holocene glacier fluctuations, Quaternary Sci. Rev., 111, 9–34, 2015.

Svendsen, L., Keenlyside, N., Bethke, I., Gao, Y., and Omrani N.-E.: Pacific contribution to the early twentieth-century warming in the Arctic, Nat. Clim. Change, 8, 793–797, https://doi.org/10.1038/s41558-018-0247-1, 2018.

Synal, H.-A., Stocker, M., and Suter, M.: MICADAS: a new compact radiocarbon AMS system, Nucl. Instrum. Methods, 259, 7–13, 2007.

Szidat, S., Salazar, G., Vogel, E., Battaglia, M., Wacker, L., Synal, H.-A., and Türler, A.: ^{14}C analysis and sample preparation at the new Bern Laboratory for the Analysis of Radiocarbon with AMS (LARA), Radiocarbon, 56, 561–566, 2014.

Tian, L., Yao, T., Wu, G., Li, Z., Xu, B., and Li, Y.: Chernobyl nuclear accident revealed from the 7010 m Muztagata ice core record, Chin. Sci. Bull., 52, 1436–1439, 2007.

Tokinaga, H., Xie, S.-P., and Mukougawa, H.: Early 20th-century Arctic warming intensified by Pacific and Atlantic multidecadal variability, P. Natl. Acad. Sci. USA, 114, 6227–6232, 2017.

Tsushima, A.: A study on reconstruction of paleo-environmental changes in the northern North Pacific region from an alpine ice core, PhD thesis, Hokkaido University, https://doi.org/10.14943/doctoral.k11790, 2015.

Uglietti, C., Zapf, A., Jenk, T. M., Sigl, M., Szidat, S., Salazar, G., and Schwikowski, M.: Radiocarbon dating of glacier ice: overview, optimisation, validation and potential, The Cryosphere, 10, 3091–3105, https://doi.org/10.5194/tc-10-3091-2016, 2016.

Walker, M., Head, M. J., Lowe, J., Berkelhammer, M., BjÖrck, S., Cheng, H., Cwynar, L. C., Fisher, D., Gkinis, V., and Long, A.: Subdividing the Holocene Series/Epoch: formalization of stages/ages and subseries/subepochs, and designation of GSSPs and auxiliary stratotypes, J. Quaternary Sci., 34, 173–186, 2019.

Winski, D., Osterberg, E., Ferris, D., Kreutz, K., Wake, C., Campbell, S., Hawley, R., Roy, S., Birkel, S., Introne, D., and Handley, M.: Industrial-age doubling of snow accumulation in the Alaska Range linked to tropical ocean warming, Sci. Rep.-UK, 7, 17869, https://doi.org/10.1038/s41598-017-18022-5, 2017.

Winski, D., Osterberg, E., Kreutz, K., Wake, C., Ferris, D., Campbell, S., Baum, M., Bailey, A., Birkel, S., and Introne, D.: A 400-Year Ice Core Melt Layer Record of Summertime Warming in the Alaska Range, J. Geophys. Res.-Atmos., 123, 3594–3611, 2018.

Yalcin, K., Wake, C. P., Kreutz, K. J., Germani, M. S., and Whitlow, S. I.: Ice core paleovolcanic records from the St. Elias Mountains, Yukon, Canada, J. Geophys. Res.-Atmos, 112, D08102, https://doi.org/10.1029/2006JD007497, 2007.

Yasunari, T. J., Shiraiwa, T., Kanamori, S., Fujii, Y., Igarashi, M., Yamazaki, K., Benson, C. S., and Hondoh, T.: Intra-annual variations in atmospheric dust and tritium in the North Pacific region detected from an ice core from Mount Wrangell, Alaska, J. Geophys. Res.-Atmos., 112, D10208, https://doi.org/10.1029/2006JD008121, 2007.

Zdanowicz, C., Fisher, D., Bourgeois, J., Demuth, M., Zheng, J., Mayewski, P., Kreutz, K., Osterberg, E., Yalcin, K., and Wake, C.: Ice cores from the St. Elias Mountains, Yukon, Canada: their significance for climate, atmospheric composition and volcanism in the North Pacific region, Arctic, 67, 35–57, 2014.

Zhang, Y. L., Perron, N., Ciobanu, V. G., Zotter, P., Minguillón, M. C., Wacker, L., Prévôt, A. S. H., Baltensperger, U., and Szidat, S.: On the isolation of OC and EC and the optimal strategy of radiocarbon-based source apportionment of carbonaceous aerosols, Atmos. Chem. Phys., 12, 10841–10856, https://doi.org/10.5194/acp-12-10841-2012, 2012.